

OMOTENASHI Trajectory Analysis and Design: Landing Phase

By Javier HERNANDO-AYUSO,¹⁾ Stefano CAMPAGNOLA,²⁾ Toshinori IKENAGA,³⁾ Tomohiro YAMAGUCHI,³⁾
Yusuke OZAWA,¹⁾ Bruno V. SARLI,⁴⁾ Shota TAKAHASHI⁵⁾ and Chit Hong YAM⁶⁾

¹⁾The University of Tokyo, Japan

²⁾JPL, USA*

³⁾JAXA, Japan

⁴⁾Catholic University of America, USA

⁵⁾Keio University, Japan

⁶⁾ispace technologies, Japan

(Received April 17th, 2017)

OMOTENASHI is a challenging mission – a lunar semi-hard lander the size of a cubesat. One of the main challenges comes from trajectory trajectory, which must be robust to execution and navigation errors. In this paper we present a detailed analysis of OMOTENASHI landing phase. We study the performance of the subsystems involved in the landing and propose a deceleration strategy. In order to assess the robustness of the trajectory, we consider uncertainties in the state vector and deceleration maneuver execution. We found that the flight path angle at Moon arrival has a great impact on the landing success rate, and it should be -10 deg or shallower. This is a very strong constraint in the design of the transfer phase trajectory. Under the current subsystems design, we found that the most critical factors are the maneuver orientation, thrust duration and total delta-v errors. Results suggest accuracy requirements to the landing devices, solid rocket motor and attitude accuracy, as well as to the transfer phase trajectory design. Finally, the errors may cause OMOTENASHI to prematurely impact against the surface during the solid rocket motor burn. This calls for a trade-off between the target final height and the maximum landing velocity.

Key Words: OMOTENASHI, Moon, Landing, Sensitivity Analysis, SLS

Nomenclature

\mathbf{r}	:	position vector
\mathbf{v}	:	velocity vector
x, y, z	:	position vector components
v_x, v_y, v_z	:	velocity vector components
α, β	:	thrust orientation angles
Δv	:	velocity increment
I_{sp}	:	specific impulse
m	:	mass
\mathbf{F}, F	:	thrust vector and magnitude
T	:	burn duration
t	:	time
h	:	height
\mathbf{u}	:	unit vector
FPA	:	Flight Path Angle
\mathbf{C}	:	covariance matrix
Subscripts		
0	:	rocket motor burn start
f	:	free-fall beginning
r	:	radial direction
s	:	transversal direction
t	:	out-of-plane direction

1. Introduction

Small satellites are being considered for missions of increasing complexity and interest. They offer a reduced cost and de-

velopment time, which allows to respond to technological and science demands in a shorter timescale. Their use in Low Earth orbit has already been proven, and there is an increasing interest on applying the concept to interplanetary missions. This was already the case of PROCYON, the first interplanetary small satellite, developed and launched by The University of Tokyo and JAXA in 2014 as a secondary payload of Hayabusa2 mission. ¹⁾ Unfortunately, PROCYON planned asteroid flyby was hindered by a failure in its main propulsion system.

One type of mission that can greatly benefit from the advantages of small satellites is Moon exploration. To this end, the use of cubesats detaching from Moon-orbiting spacecraft has been proposed in the past. ²⁾ However if a piggyback opportunity in a mission that features a lunar flyby is available, the mission scenario simplifies considerably.

This opportunity will arise in the first launch of American Space Launch System (SLS), called Exploration Mission-1 (EM-1). After launch in late 2018, thirteen 6U cubesats will be injected into a lunar flyby orbit. ³⁾ The University of Tokyo and JAXA will seize this opportunity with OMOTENASHI (Outstanding Moon exploration Technologies demonstrated by NanoSemi-Hard Impactor). OMOTENASHI mission seeks to study the lunar surface's radiation environment and soil mechanics using a nano-lander. ⁴⁾ However OMOTENASHI is a challenging mission. One of the main challenges comes from trajectory trajectory, which must be robust to execution and navigation errors. As we present in this paper, a robust trajectory must have a small flight path angle (FPA) at Moon arrival. In particular, we found that it must satisfy $-7 \text{ deg} \leq FPA \leq 0 \text{ deg}$ in order to be error-robust. To this end, the design of the trans-

* The work of Stefano Campagnola was carried out as an International Top Young Fellow in ISAS/JAXA, Japan

fer and the landing phases cannot be performed independently, as they are strongly coupled.

After detaching from SLS, OMOTENASHI must perform two deterministic maneuvers that will make this cubesat the first one to perform a semi-hard landing on the Moon. A first maneuver, DV1, will inject OMOTENASHI into a Moon-impacting orbit. After performing midcourse trajectory correction maneuvers (TCM) as needed, a solid rocket motor will be ignited shortly before the expected Lunar surface collision at a speed of approximately 2.5 km/s. After the deceleration maneuver (DV2), OMOTENASHI will experience a free-fall from a low height (close to 100 m) and arrive at the Moon surface with a speed of around 20 m/s.^{4,5} In order to reduce the mass budget, OMOTENASHI is composed of an orbital module, a deceleration module and a landing module. The orbital module will be ejected at rocket motor ignition, and the landing module will separate from the deceleration module at burnout.

In this paper we perform a detailed analysis of the landing phase and the DV2 maneuver. We study the subsystems performance and propose a deceleration strategy based on targeting a final height with zero vertical velocity. We consider uncertainties in the initial state (Orbit Determination - OD) and maneuver execution (attitude and propulsion) in order to assure the robustness of the trajectory. Results provide the range of acceptable FPA that lead to a safe landing. Critical error sources are identified, and requirements to the involved subsystems are also deduced from the simulations. We show how improving the accuracy of the critical factors improves the landing success rate.

2. Trajectory overview

SLS maiden flight EM-1 will deliver 13 satellites into a Moon fly-by orbit, being OMOTENASHI one of them. The deployment trajectory must be modified to target a lunar-impact trajectory that leads to a safe landing. To do so, OMOTENASHI must operate its cold gas thrusters as early as possible, as the required fuel consumption increases with time. However system health checks and OD need to be performed before the spacecraft can maneuver. As a compromise, the first maneuver DV1 is planned at 24 hours after deployment. If necessary, a trajectory correction maneuver will be performed 24 hours after DV1 to compensate for DV1 execution errors. Detail design of Earth-Moon transfer robust trajectories is presented in Ref. 6. During the landing phase, OMOTENASHI will ignite its solid rocket motor to decelerate about 2.5 km s^{-1} . To achieve this, the orbital module will detach after ignition to reduce mass and only the rocket motor and the payload will be slowed down. After burnout, the payload will separate from the rocket motor and free-fall onto the Moon surface from a height close to 100 m. An overview of the complete trajectory is shown in Fig. 1.

In the absence of trajectory errors, any Moon-impacting trajectory could be employed in OMOTENASHI mission. However when navigation and execution errors are considered, the set of feasible trajectories is greatly reduced. We find that the transfer phase is must lead to a small FPA at Moon arrival to provide robustness to DV2 execution errors. If this was not the case small delays in the execution of the deceleration maneuver would lead to unacceptable displacements in the vertical direc-

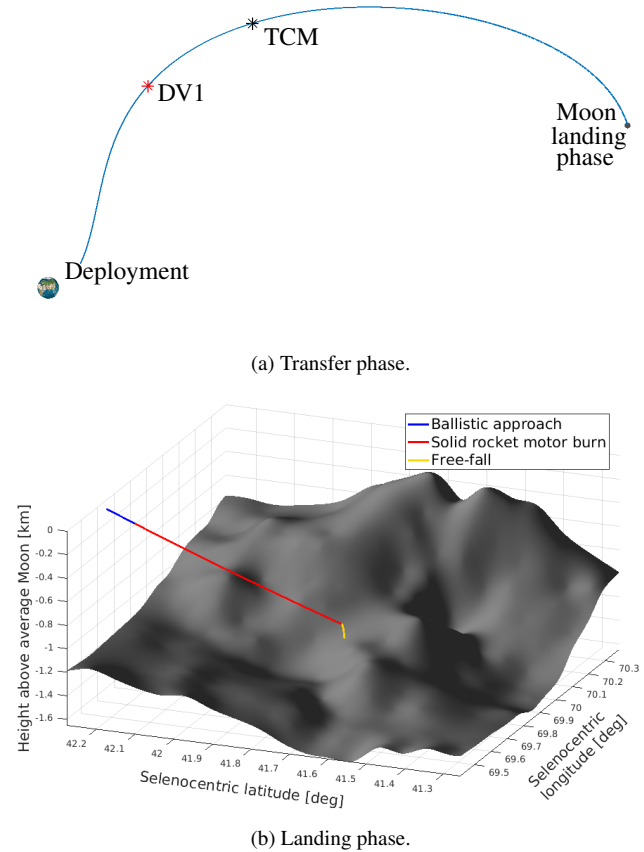


Fig. 1. Trajectory overview.

tion, potentially causing the landing to occur at excessively high speeds. However a very small FPA results in a strong constraint in the design of the transfer phase, as the navigation and DV1 executions errors may lead to a Moon flyby. Note that even in this scenario OMOTENASHI could land by using its rocket motor near perilune, but the resulting landing velocity would likely be higher than the design value. On the other hand, errors in the transfer phase may also induce a steep FPA that could jeopardize the landing. Consequently, the transfer phase design is strongly coupled with the landing phase of OMOTENASHI.

The current analysis was conducted with the initial conditions provided by Marshall Space Flight Center⁷⁾ and shown in Table 1. The position and velocity components are expressed in a Moon-centered reference frame whose axes are parallel to the J2000 Ecliptic frame. The candidate DV1 maneuvers, which were chosen following the results of the transfer phase preliminary analysis and a linearized landing study, are characterized in Table 2. They cover a wide range of possible trajectories that could potentially lead to a safe landing. The azimuth angle is defined as the angle between the x axis and the projection of DV1 onto the $x-y$ plane, and the polar angle is defined as the angle between the z axis and DV1. All the candidate DV1 maneuvers are performed at epoch 2018 Oct 08 15:39:16, which corresponds to one day after separation from SLS. The analysis was performed considering the Sun, Earth and Moon Gravity and an impulsive DV1 maneuver. In the future solar radiation pressure, spherical harmonics and finite burns will be included, but the results will not qualitatively change.

Table 1. Initial conditions expressed in the Moon-centered J2000 Ecliptic frame.

Component	value
Epoch	2018 Oct 07 15:39:16
x [km]	341 095.06
y [km]	-43 570.46
z [km]	-18 326.52
v_x [km s ⁻¹]	-3.59
v_y [km s ⁻¹]	-2.71
v_z [km s ⁻¹]	0.98

Table 2. Candidates DV1 maneuvers. The angles are defined with respect to the Moon-centered J2000 Ecliptic frame.

case	Δv [m s ⁻¹]	azimuth [deg]	polar angle [deg]	FPA at Moon arrival [deg]
1	15	63.84	45.38	-2.5
2	15	63.94	45.56	-3.6
3	15	72.09	45.28	-4.8
4	15	64.59	46.13	-5.9
5	15	63.75	46.5	-6.9
6	15	63.75	47.1	-8.0

3. Moon topography model

The lunar terrain is modeled using high resolution data provided by the SELENE mission. SELENE topographical data features an angular resolution of 1/16 deg and an accuracy of 5 m.⁸⁾ This model allows the trajectory team to evaluate the height over an average Moon of radius 1734.4 km for any point on the lunar surface. A comparison of the surface provided by this model with real Moon surface photographs is provided in Fig. 2.

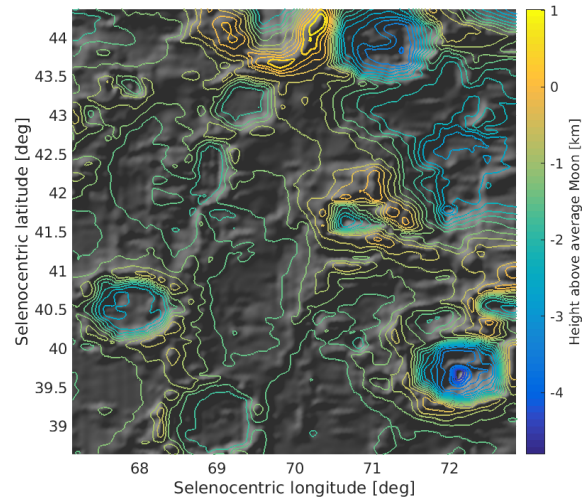
The use of a real surface model is critical for OMOTENASHI mission success. If a simple spherical surface model for the Moon was chosen, the terrain elevation would not be correctly assessed and the spacecraft would arrive at the Moon surface at an structurally unacceptable velocity.

4. Orbit determination

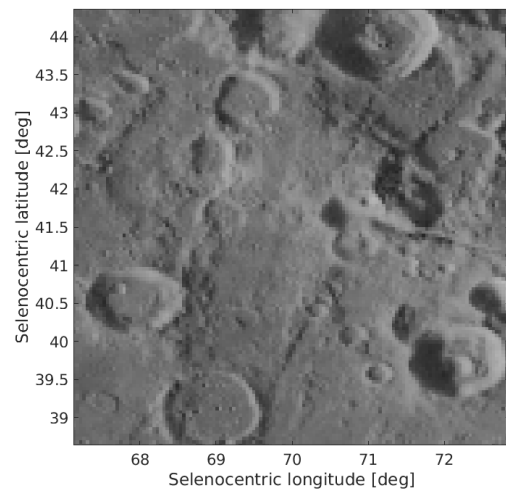
Orbit Determination accuracy plays a critical role in the safety of the landing. The vertical position error should be much smaller than the free-fall initial height in order to avoid catastrophic landings. Additionally, orbit delays could also jeopardize the final part of the mission, even if the approach trajectory has a small FPA.

A first OD analysis was performed using only JAXA resources to decrease the mission cost and complexity. To this end, a campaign of observations (see Table 3) from Uchinoura Space Center (USC) was planned and simulated using an in-house software tool. In the simulation, a priori covariance was not considered. The visibility from the USC ground station and the communication windows are shown in the upper part of Fig. 3. During the last communication window no OD is planned, as a cut-out time for final tuning and uplink of DV2 is introduced. The simulated covariance matrix at DV2 epoch provides a vertical error close to 400 m, unacceptable for a safe landing with a free-fall initial height of around 100 m.

After studying several configurations, it was decided to



(a) Surface model and isoheight curves.



(b) Photography of the Moon surface.

Fig. 2. Comparison between SELENE surface model and Moon surface photographs in the landing location of the candidate trajectories.

include Delta Differential One-way Ranging (delta-DOR or DDOR) measurements using the NASA Deep Space Network (DSN) stations in Goldstone (GDS), Canberra (CAN) and Madrid (MAD). This method requires two stations to be visible at the same time, and can be accomplished with the combinations GDS-CAN and CAN-MAD as can be seen in Fig. 3. The measurements are characterized by the lower row of Table 3. Results show a vertical 3-sigma error of the order of 50 m, which will not jeopardize the landing maneuver as it will be shown later. The position covariance matrix at the solid rocket motor ignition, expressed in the J2000 Ecliptic reference system and in km², is:

$$C_0 = \begin{bmatrix} 1.30 \times 10^{-3} & -9.70 \times 10^{-4} & 1.70 \times 10^{-3} \\ -9.70 \times 10^{-4} & 7.20 \times 10^{-4} & -1.30 \times 10^{-3} \\ 1.70 \times 10^{-3} & -1.30 \times 10^{-3} & 2.40 \times 10^{-3} \end{bmatrix} \quad (1)$$

5. Braking maneuver design

The solid rocket motor is at an early phase of design and its thrust profile is not fully available yet. Consequently, the thrust

Table 3. Orbit Determination observables.

type	duration	interval	1- σ noise	bias	number of observations
X-band 2-way Doppler	3 h	60 s	0.5 mm s ⁻¹	no bias	3 if TCM, 4 otherwise
X-band 2-way range	30 min	60 s	10 m	no bias	3 if TCM, 4 otherwise
DDOR (GDS-CAN, CAN-MAD)	30 min	600 s	1 ns	no bias	4 (only if using non-JAXA stations)

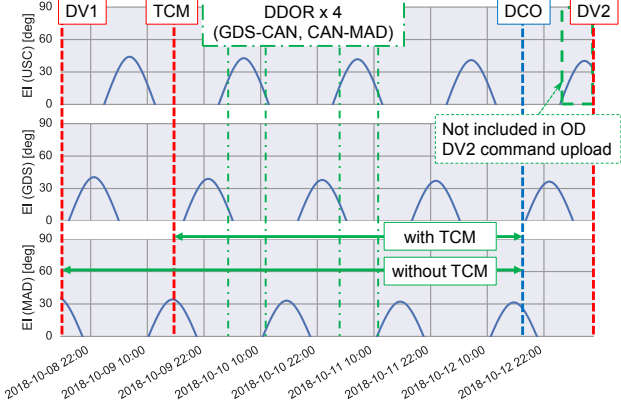


Fig. 3. Ground station visibility and observations planning. CAN is omitted as the visibility is similar to USC.

is modeled as constant through the total duration of the burn. If the velocity increment Δv , the specific impulse I_{sp} , the burn duration T , and the initial spacecraft mass m_0 are known, the thrust magnitude F can be determined as

$$F = \frac{m_0 \left(1 - \exp\left(-\frac{\Delta v}{I_{sp}}\right) \right)}{T} I_{sp}. \quad (2)$$

Moreover, we assume that the thrust is applied along an inertially-fixed direction. To give this orientation, we introduce the Local-Vertical Local-Horizontal reference frame (LVLH) $\langle \mathbf{u}_r, \mathbf{u}_s, \mathbf{u}_t \rangle$ of the OMOTENASHI Selenocentric orbit at the burn start epoch. Its axes are given by the unit vectors aligned with the radial direction \mathbf{u}_r , the out-of-plane direction \mathbf{u}_t and the transversal direction \mathbf{u}_s :

$$\mathbf{u}_r = \frac{\mathbf{r}}{\|\mathbf{r}\|_{t_0}}, \quad \mathbf{u}_t = \frac{\mathbf{v} \times \mathbf{r}}{\|\mathbf{v} \times \mathbf{r}\|_{t_0}}, \quad \mathbf{u}_s = \mathbf{u}_r \times \mathbf{u}_t \quad (3)$$

With this convention, the local vertical plane is defined by the unit vectors \mathbf{u}_r and \mathbf{u}_s , and the local horizontal plane is defined by the unit vectors \mathbf{u}_s and \mathbf{u}_t . The thrust direction is determined by the angle with respect to the local horizontal plane α and the angle with respect to the local vertical plane β :

$$\mathbf{F} = F \left(\cos \beta \sin \alpha \mathbf{u}_r + \cos \beta \cos \alpha \mathbf{u}_s - \sin \beta \mathbf{u}_t \right) \quad (4)$$

After the solid rocket motor parameters have been fixed, the design of the breaking maneuver has three degrees of freedom: the orientation angles α and β , and the motor ignition time t_0 . In the first place the out-of-vertical-plane angle β is set to 0, otherwise the deceleration effectiveness would be reduced and the residual final-velocity would increase. To fix the two remaining variables, we impose two constraints at the motor burn-out: zero vertical velocity and a target height h_f over the Moon surface. With these constraints, the design problem is mathematically closed and the maneuver parameters can be calculated. The DV2 design parameters are summarized in Table 4.

Table 4. DV2 parameters.

Design parameter	Nominal value
t_0	fixed by free-fall condition
α	fixed by free-fall condition
β	0 deg
I_{sp}	260 s
Δv	2.5 km s ⁻¹
T	20 s

The final landing velocity depends on the residual horizontal velocity, the target height and the local topography. This velocity is limited by requirements of the impact absorption mechanisms. Current design suggests a limit of 30 m s⁻¹ for the components of the velocity parallel and perpendicular to the ground.⁹⁾

6. Maneuver execution error

Errors in the deceleration maneuver execution may cause OMOTENASHI to deliver the payload to the lunar surface at an unacceptable velocity. Unless otherwise specified, all the errors are assumed to follow Gaussian distributions.

In the first place, the solid rocket motor ignition could happen with a delay with respect to the design ignition time. This includes both onboard clock errors and ignition delays. The former are estimated to smaller than 0.01 s, while the latter are estimated to be about 0.1 s. These errors, together with OD error, demand a shallow FPA when approaching the Moon to minimize the vertical position error.

Next, the solid rocket engine could show performance outside its design point. In particular we consider variations in the specific impulse and thrust duration, caused by a different combustion rate and non-uniformities in the solid fuel. Additionally, initial fuel mass errors or left-over fuel will lead to a different total Δv .

Another important factor is to consider the errors on the thrust direction. OMOTENASHI will be spin-stabilized during the deceleration maneuver, being the accuracy of the spin axis of about 1 deg. The spin axis can also nutate due to perturbations, caused by the initial spin state and the separation of the orbital module right after ignition and perturbations during the motor burn. This effect will average over a nutation period and is modeled by a penalty on the total Δv . This penalty consists of a negative half-normal Gaussian distribution whose 3- σ standard deviation is equal to a 2% of the total Δv .

The execution errors and its values are summarized in Table 5.

7. Sensitivity analysis

In order to assess the robustness of the landing phase, we performed an extensive campaign of Monte-Carlo (MC) simula-

Table 5. Maneuver execution errors.

Design parameter	3σ error
t_0	± 0.11 s
α	± 1 deg
β	± 1 deg
I_{sp}	± 5 s
Δv	$\begin{cases} \pm 25 \text{ m s}^{-1} \\ -50 \text{ m s}^{-1}(\text{nutation}) \end{cases}$
T	± 2 s

tions with $n_{MC} = 10^3$ points, sampling from the N-dimensional Gaussian distribution that includes the N sources of error, and propagating the orbit until OMOTENASHI lands on the real Moon surface. To test different scenarios, the initial free-fall height was selected as $h_f = \{80, 130, 180, 230\}$ m.

Figure 4 reveals that for a non-negligible portion of the MC samples and for all the considered heights and FPAs, OMOTENASHI makes contact with the lunar surface during the solid rocket motor burn.

For the MC samples that arrive at the Moon surface after the motor burnout, we projected the landing velocity into the local ground-tangent and normal directions using the local Moon topography. Figure 5 shows the impact normal velocity cumulative distribution function (cdf), and reveals a landing success rate between 40% and 65% for all the considered heights and cases. The success rate could be greatly improved if a higher impact velocity was admissible, and the free-fall height was augmented. The advantages of a trajectory with a shallow FPA is also clear in Fig. 5, as the landing success rate is higher than for deeper FPA trajectories. A trade-off involving the transfer and the landing phase will determine the FPA of the final trajectory. Finally, Fig. 6 shows the impact ground-tangent velocity cdf for the different initial heights. The ground-tangent velocity decreases as the free-fall initial height increases, which suggests that the deceleration maneuver is less efficient if the target final height is low. If only the ground-tangent velocity was important, one should aim for a higher initial height than the values we considered.

To assess the importance of each source of error, the analysis performed above with the full error model was repeated for case 2 ($FPA = -3.6$ deg), considering only one error source is acting per simulation. For each MC run, the standard deviations of the ground-tangent and normal impact velocities were calculated. Table 6 shows the $3\text{-}\sigma$ values of the normal impact velocity. It reflects the strong influence of the out-of-horizontal-plane angle α and the burn duration T on the landing dispersion. Table 7 shows the $3\text{-}\sigma$ values of the ground-tangent impact velocity: the dispersion is governed by the DV2 magnitude and the out-of-vertical-plane angle β .

From these results, one may infer that in order to increase the success rate of the landing phase, one or several of the following strategies could be considered:

1. Increase the structural limit of the landing devices. This would allow to raise the initial free-fall height, and would decrease the number of premature landings and augment the probability of the landing velocity to be in the feasible range.
2. Improve the attitude accuracy during the solid rocket en-

gine burn. In this way, the efficiency of the deceleration maneuver would be increased.

3. Improve the solid rocket engine performance. This would also lead to a more efficient deceleration maneuver

All of these options are under study by the OMOTENASHI team, carefully trading-off the increased cost and complexity for every subsystem with the accepted mission risk.

If these critical factors were improved, the landing success rate would highly increase. To illustrate it, we chose a scenario in which for case 2 ($FPA = -3.6$ deg) the critical errors (α , β , T , and Δv – both magnitude and nutation effect) were cut by half. The rest of the errors were unchanged with respect of the previous simulations. Results are shown in Figs. 7 and 8, and an overall improvement can be observed. The success rate is above 80%, and if the landing velocity structural limit is raised to 40 m s^{-1} it increases well over 95%.

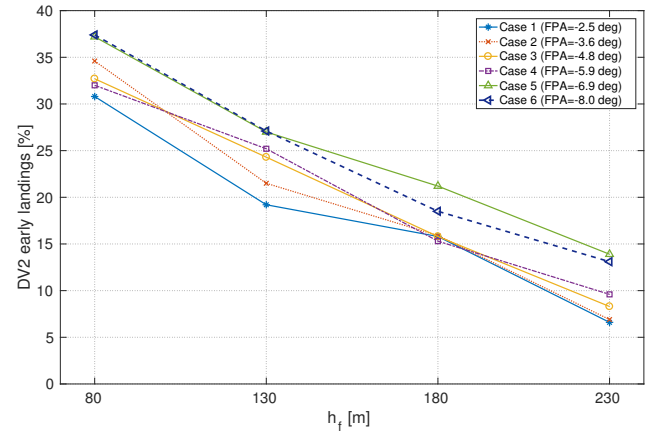


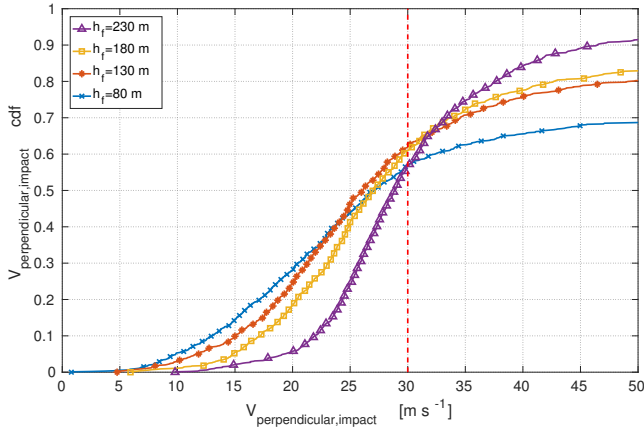
Fig. 4. Premature landings during solid rocket motor under the full error model.

Table 6. Normal landing velocity $3\text{-}\sigma$ variation [m s^{-1}]

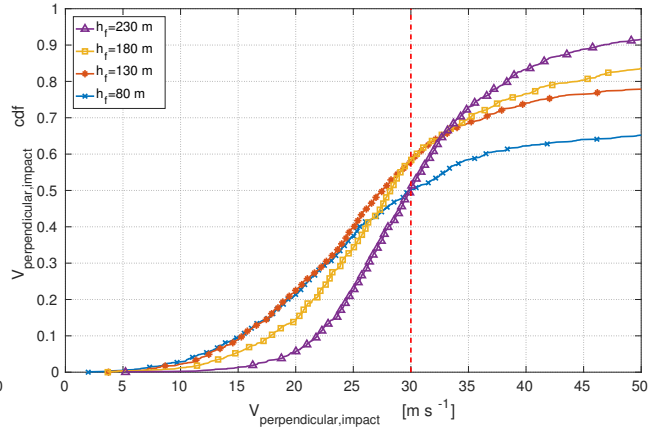
h_f	80 m	130 m	180 m	230 m
all errors	29.67	26.77	26.05	24.69
OD only	5.86	4.77	3.98	3.12
t_0 only	3.26	2.50	2.14	1.16
α only	28.15	25.31	22.03	22.74
β only	1.64	1.03	0.64	0.60
I_{sp} only	0.85	0.64	0.57	0.30
Δv only	3.04	2.67	2.42	1.03
T only	20.18	19.80	18.49	15.63

Table 7. Ground-tangent landing velocity $3\text{-}\sigma$ variation [m s^{-1}]

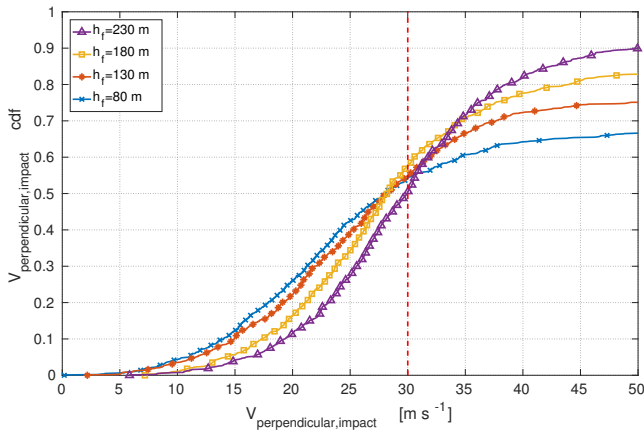
h_f	80 m	130 m	180 m	230 m
all errors	38.33	38.34	37.26	37.33
OD only	0.20	0.17	0.14	0.12
t_0 only	0.09	0.06	0.05	0.02
α only	1.53	1.83	2.05	2.37
β only	18.18	17.30	19.15	18.41
I_{sp} only	0.02	0.02	0.01	0.01
Δv only	38.11	38.39	39.04	38.81
T only	0.52	0.50	0.46	0.37



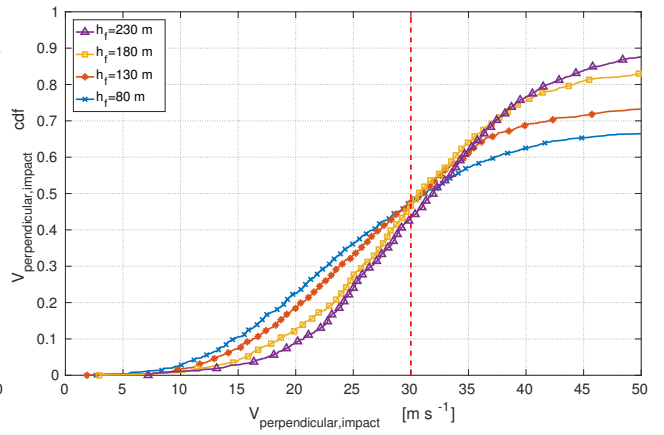
(a) Case 1 ($FPA = -2.5$ deg).



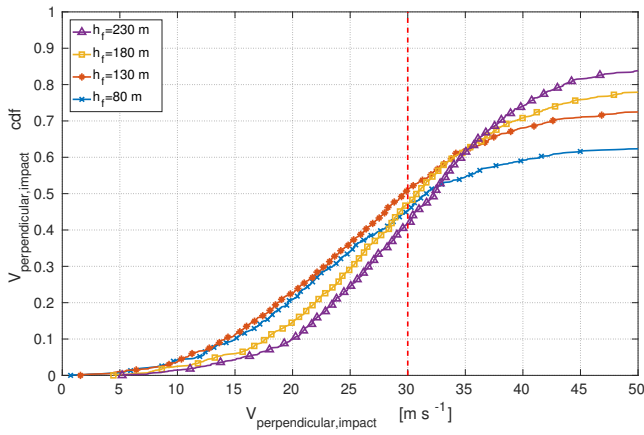
(b) Case 2 ($FPA = -3.6$ deg).



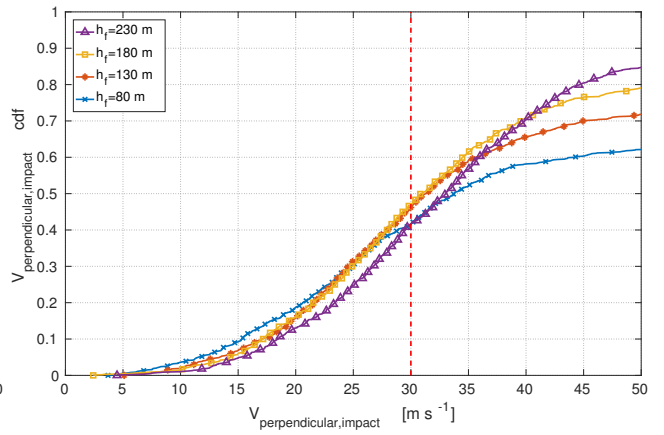
(c) Case 3 ($FPA = -4.8$ deg).



(d) Case 4 ($FPA = -5.9$ deg).

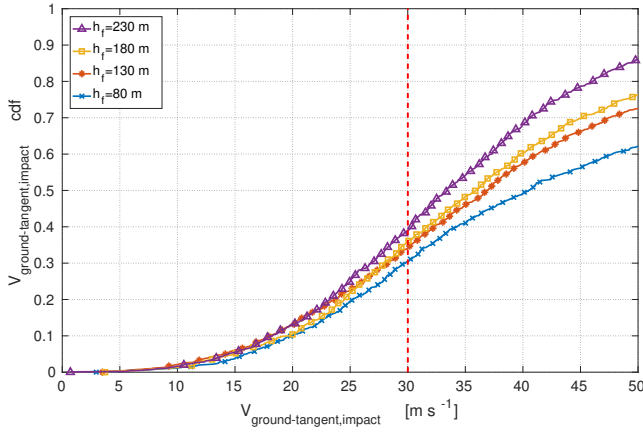


(e) Case 5 ($FPA = -6.9$ deg).

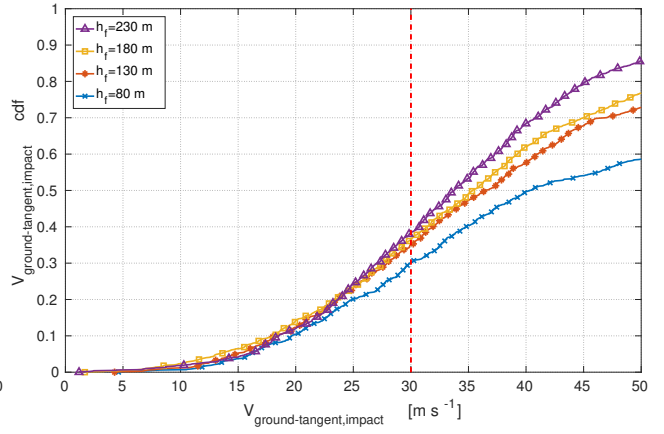


(f) Case 6 ($FPA = -8$ deg).

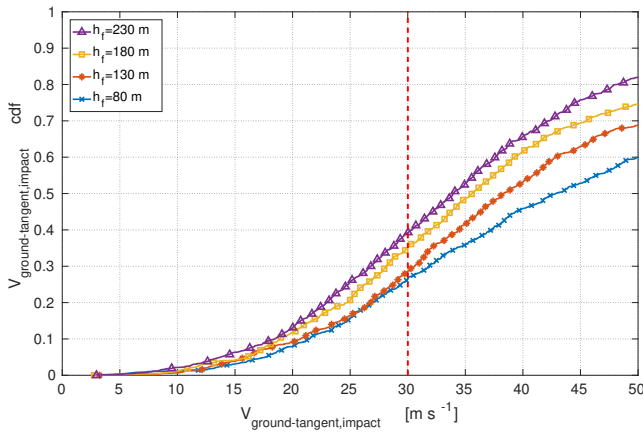
Fig. 5. Normal impact velocity cdf considering the full error model.



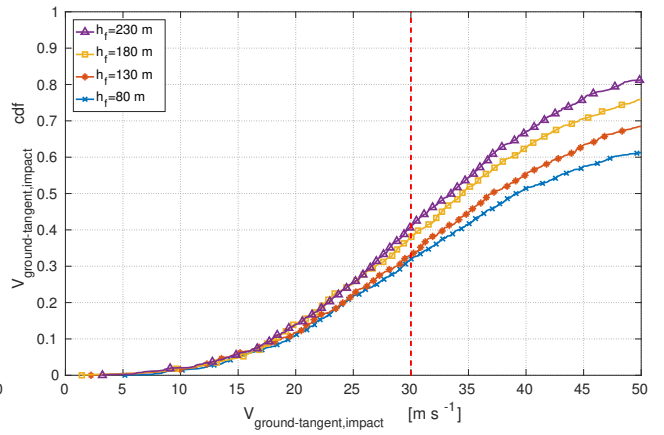
(a) Case 1 ($FPA = -2.5$ deg).



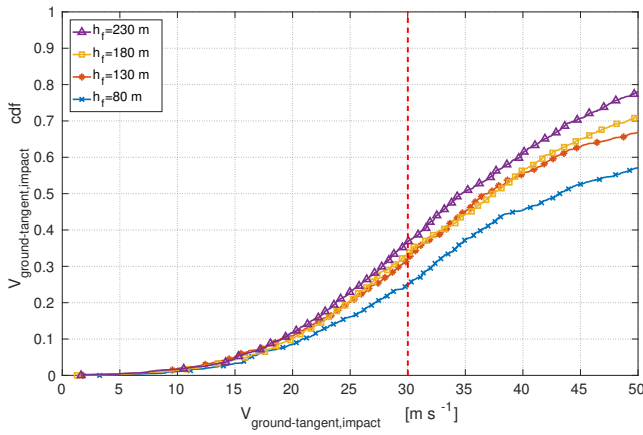
(b) Case 2 ($FPA = -3.6$ deg).



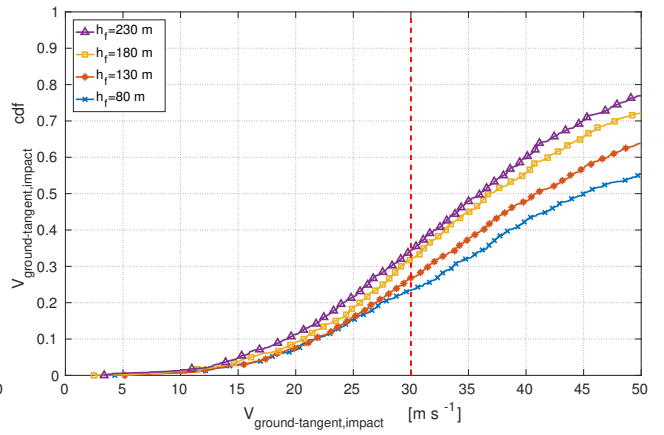
(c) Case 3 ($FPA = -4.8$ deg).



(d) Case 4 ($FPA = -5.9$ deg).



(e) Case 5 ($FPA = -6.9$ deg).



(f) Case 6 ($FPA = -8$ deg).

Fig. 6. Ground-tangent impact velocity cdf considering the full error model.

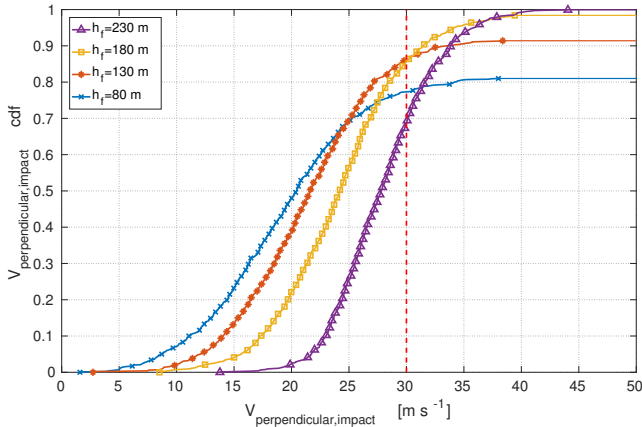


Fig. 7. Normal impact velocity cdf with improvement on critical errors ($FPA = -3.6$ deg).

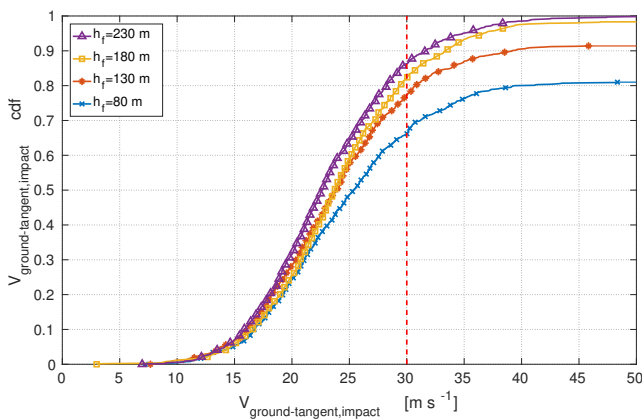


Fig. 8. Ground-tangent impact velocity cdf with improvement on critical errors ($FPA = -3.6$ deg).

8. Conclusion

In this paper the current state of the landing phase of OMOTENASHI mission was presented. A deceleration maneuver using a solid rocket motor, reaching a final zero vertical-velocity and a specified height over the Moon surface, will be followed by a ballistic free-fall.

All error sources were identified and characterized. Deviations from the nominal trajectory were studied and the most critical contributions were determined, which in turn allows to propose requirements to the design of the related subsystems in order to increase the landing success rate.

Simulation results identify several critical factors that could be improved in order to increase the landing success rate: struc-

Acknowledgments

The Ministry of Education, Culture, Sports, Science and Technology (MEXT) of the Japanese government supported tural limit of the landing devices and accuracy of attitude and solid rocket engine. This is currently being considered by OMOTENASHI team.

The effect of the flight path angle at Moon arrival was also studied. It was found that for this kind of mission it is necessary to design a shallow flight path angle trajectory, shallower than -7 deg. This imposes constraints on the design of the transfer phase, which becomes strongly coupled with the landing phase.

Javier Hernando-Ayuso under its program of scholarships for graduate school students.

References

- 1) Funase, R., Koizumi, H., Nakasuka, S., Kawakatsu, Y., Fukushima, Y., Tomiki, A., Kobayashi, Y., Nakatsuka, J., Mita, M., Kobayashi, D. et al.: 50kg-class deep space exploration technology demonstration micro-spacecraft PROCYON, *Small Satellite Conference*, Utah, USA, 2014.
- 2) Song, Y.-J., Lee, D., Jin, H. and Kim, B.-Y.: Potential trajectory design for a lunar CubeSat impactor deployed from a HEPO using only a small separation delta-V, *Advances in Space Research*, **59(2)** (2017), pp. 619–630.
- 3) Schorr, A. A. and Creech, S. D.: Space Launch System Spacecraft and Payload Elements: Making Progress Toward First Launch (AIAA 2016-5418), *AIAA SPACE 2016*, 2016.
- 4) Hashimoto, T., Yamada, T., Kikuchi, J., Otsuki, M. and Ikenaga, T.: Nano Moon Lander: OMOTENASHI, *31st International Symposium on Space Technology and Science*, 2017-f-053, Matsuyama, Japan, 2017.
- 5) Campagnola, S., Ozaki, N., Hernando-Ayuso, J., Oshima, K., Yamaguchi, T., Ikenaga, T., Yam, C. H., Oguri, K., Kakihara, K., Takahashi, S., Ozawa, Y., Ferella, L., Funase, R. and Hashimoto, T.: Nano Moon Lander: OMOTENASHI, *31st International Symposium on Space Technology and Science*, 2017-f-044, Matsuyama, Japan, 2017.
- 6) Ozawa, Y., Takahashi, S., Hernando-Ayuso, J., Campagnola, S., Ikenaga, T., Yamaguchi, T. and Sarli, B.: OMOTENASHI Trajectory Analysis and Design: Earth-Moon Transfer Phase, *31st International Symposium on Space Technology and Science*, Matsuyama, Japan, 2017.
- 7) Stough, R.: REVISED - Delivery of Interim October 7th 2018 Launch Post ICPS Disposal State Vectors for Secondary Payload Assessment, Technical report, George C. Marshall Space Flight Center, NASA, 2016.
- 8) Araki, H., Tazawa, S., Noda, H., Ishihara, Y., Goossens, S., Sasaki, S., Kawano, N., Kamiya, I., Otake, H., Oberst, J. and Shum, C.: Lunar Global Shape and Polar Topography Derived from Kaguya-LALT Laser Altimetry, *Science*, **323(5916)** (2009), pp. 897–900.
- 9) Yamada, T., Tanno, H. and Hashimoto, T.: Development of Crushable Shock Absorption Structure for OMOTENASHI Semi-hard Impact Probe, *31st International Symposium on Space Technology and Science*, ISTS-2017-f-055, Matsuyama, Japan, 2017.